Inorganic Chemistry

pubs.acs.org/IC Article

A Complex Spin-Transition Thermal Hysteresis Unlocked by Two Competing Symmetry-Breakings

Published as part of Inorganic Chemistry special issue "Pushing the Limits of Molecular Magnetism".

Maryam Alashoor, Ricardo G. Torres Ramírez, Olaf Stefanczyk, Kazuki Nakamura, Francisco Javier Valverde-Muñoz, Elzbieta Trzop, Ivan da Silva, Shin-ichi Ohkoshi, Arnaud Grosjean, Nathalie Daro, Philippe Guionneau, Laurent Guérin,* and Eric Collet*

Cite This: *Inorg. Chem.* 2026, 65, 19485−19494 Read Online

ACCESS | Metrics & More | Article Recommendations

ABSTRACT: The spin-crossover material $[Fe(NH_2trz)_3](NO_3)_2$ belongs to the class of 1D triazole-based polymeric SCO complexes. It exhibits a thermal phase transition, with a 28 K wide thermal hysteresis, characterized by phase transition temperatures $T_{\uparrow}$ = 346 K upon warming and $T_{\downarrow}$ = 318 K upon cooling. This hysteretic thermal phase transition is unusual because it is associated with two competing symmetry-breaking phenomena: a ferroelastic distortion upon warming from the low-spin (LS) trigonal phase to the high-spin (HS) triclinic phase, and a unit cell tripling upon cooling from the HS phase to the LS phase. Magnetic, spectroscopic and X-ray diffraction measurements reveal a clear coupling between the spin transition and the two competing symmetry changes. Since there is no group-subgroup relationship between the LS and HS phases, the phase transition can only be discontinuous. However, the detailed analysis shows that the situation is more complex, since both LS and HS phases are two daughter phases of a parent high-symmetry phase. The phase transitions are then rationalized within the frame of our theoretical model based on the Landau theory of phase transitions, which considers the coupling of the spin transition to both types of competing symmetry-breakings between the LS and HS phases. The theoretical approach reproduces the experimental findings and explains the origin of this hysteretic spin transition.

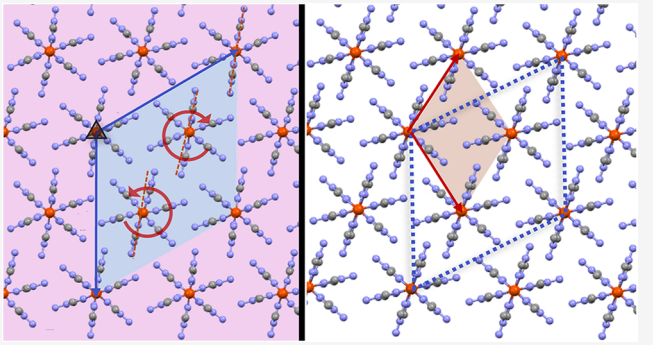

INTRODUCTION

Spin-crossover (SCO) Fe(II)-based molecular complexes represent a key class of materials that may exhibit bistability between the paramagnetic high-spin (HS, S = 2, t_{2g}^4 e_g^2) and diamagnetic low-spin (LS, S = 0, t_{2g}^6 e_g^0) electronic configurations.[1−3] Since these states differ in entropy, volume and electronic configurations, they can be switched by the application of diverse external stimuli such as temperature, pressure, light irradiation or magnetic field. Among these materials, triazole-based polymeric compounds, $[Fe(R\text{-}trz)_3]X_2$ (where R-trz = triazole stands for 4-R-substituted-1,2,4-triazole, and X as a counteranion to compensate the positive charge of the polymeric chain), have attracted special attention because they were initially depicted, already three decades ago, as one of the most promising SCO materials for memory devices.[4] Nowadays, SCO materials are again cited as ideal systems for some technological applications, such as solid-state cooling barocaloric devices, and ultrafast photoinduced spin state switching.[5−9]

Generally, these one-dimensional (1D) polymeric Fe(II) materials undergo cooperative thermally induced LS-to-HS transitions near room temperature and usually exhibit a large thermal hysteresis, associated with a reversible white-to-pink color change.[10] Triazole-based materials occupy a special place among SCO molecular compounds in that they crystallize into distinct parallel chains that interact with one another via anionic groups and, possibly, solvent molecules. Crystallizing these materials into single crystals is a significant challenge, rarely achieved, and when it is, it occurs randomly and is not very reproducible. It was the fortuitous isolation of single crystals of the compound $[Fe(NH_2trz)_3](NO_3)_2$ that, after more than two decades of attempts, made it possible to use

Received: June 8, 2026
Revised: July 29, 2026
Accepted: August 3, 2026
Published: August 10, 2026

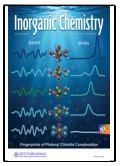

https://doi.org/10.1021/acs.inorgchem.6c02968
Inorg. Chem. 2026, 65, 19485−19494

single-crystal X-ray diffraction[11] to definitively reveal and confirm the earlier structural models for $[Fe(R\text{-}trz)_3]X_2$ compounds, based on other complementary techniques during the investigation of crystalline powders.[12−17] This reference crystal structure provides a foundation for all subsequent and current structural investigations of these 1D SCO materials, including those performed on powder, such as the one carried out here.

In many cases, the entropy-driven SCO phenomenon is an isosymmetric process,[1,2,8,18−21] where the symmetry is unchanged. These more or less cooperative thermal conversions, from LS to HS states, are monitored through the thermal evolution of the SCO parameter $q = \frac{N_{HS} - N_{LS}}{N_{HS} + N_{LS}}$, where N_{LS} and N_{HS} refer to the number of active iron centers in each state. q is totally symmetric, as it belongs to the identity representation, and its coupling to the volume strain is responsible for cooperative spin state conversion.[22] Moreover, the effect of the coupling of the SCO phenomenon with symmetry-breaking, related to Jahn−Teller distortion, ferroelastic phase transition and/or spin-state ordering, gives rise to important and interesting features, such as stepwise SCO, and it influences hysteretic behaviors in terms of broadening and shape.[23−32] This coupling is of great interest for extending the field of application of SCO materials, as it opens the way for magnetoelectric effects or symmetry-breaking upon warming for example.[33,34] These phenomena were recently rationalized within the framework of a theoretical model developed by Collet, based on the Landau theory of phase transitions, and considering the lattice-mediated elastic coupling of the SCO with symmetry-breaking.[22,35−37] In the Landau-based studies reported so far, the symmetry change was always associated with a group-subgroup relationship between the LS and HS phases. Here we show that this is not the case for the $[Fe(NH_2trz)_3](NO_3)_2$ complex, as two competing symmetry-breaking phenomena occur: a unit cell tripling upon cooling and a ferroelastic distortion upon warming. Our symmetry analysis reveals that the LS and HS phases are two distinct daughter phases of a common higher-symmetry parent phase. We successfully describe with our Landau-based model the hysteretic and concomitant spin transition and symmetry changes in $[Fe(NH_2trz)_3](NO_3)_2$.

EXPERIMENTAL SECTION

Synthesis and Characterization

The $[Fe(NH_2trz)_3](NO_3)_2$ powder used for measurements was obtained by adapting a reported procedure,[38] from aqueous solutions of iron(II) nitrate (0.33 mol L^{-1}) and 4-amino-1,2,4-triazole (1 mol L^{-1}) at 60 °C. Iron(II) nitrate was prepared by the exchange reaction between $FeSO_4$ and $Ba(NO_3)_2$ and without being isolated from the solution. The resulting purple precipitate was washed with ethanol and dried in the air. Anal. Calc. for $C_6H_{12}FeN_{14}O_6{\cdot}0.5H_2O$ (M_W = 441.1 g mol^{-1}): Fe 12.6%, C 16.3%, H 3.0%, N 44.5%; Found: Fe 12.0%, C 16.3%, H 2.8%, N 44.0%. In agreement with the elemental analysis, the thermogravimetric experiments performed on the powder are consistent with the presence of 0.5 molecule of water (2.0%).

Variable temperature magnetic data for the powder samples were collected using a Quantum Design MPMS-5S magnetometer (San Diego, CA) under a field of 5000 Oe. Measurements were performed between 260 and 380 K (heating and cooling mode) every 2 K with a scan rate of 0.5 K min^{-1} on a powder sample prepared in a gelatin capsule. The methodology used to measure the magnetic behaviors within the SCO research community follows standardized practices that are essential for a meaningful comparison of the observed phenomena.[39]

Ultraviolet−Visible (UV−vis) absorption spectra were measured using a Shimadzu UV-3600 plus spectrometer with an Oxford Instruments Microstate-He cryostat. For the measurements, the sample was dispersed in paraffin oil and sandwiched between quartz plates.

Powder X-ray Diffraction Studies

We studied the structural evolution upon heating and cooling by powder X-ray diffraction using a Rigaku Ultima-IV diffractometer, equipped with Cu Kα source (λ = 1.5418 Å). We also collected high-resolution powder X-ray diffraction data at the CRISTAL beamline of the Synchrotron SOLEIL, using a 2-circle diffractometer equipped with a curved pixel detector built with 9 Dectris Mythen II modules and positioned on a cylinder with a radius of 720 mm. The powder sample was packed in a 0.5 mm diameter capillary, and it was kept under continuous rotation around its longitudinal axis during the data acquisition. The energy of the X-ray beam was adjusted to 17 keV (0.7296 Å), calibrated with a LaB_6 standard sample (NIST-SRM660). We used the TOPAS software[40] for data analysis. The detailed structural analysis will be presented in another paper, where the intramolecular reorganization will be compared in detail with density functional theory (DFT) calculations to explain the microscopic origin of the Jahn−Teller distortion and changes in interchain interactions. Here we focus our attention on the symmetry changes of the lattice (distortion and periodicity) based on the powder X-ray diffraction data analysis.

RESULTS AND DISCUSSION

Spin-Transition Thermal Hysteresis Analysis

The $[Fe(NH_2trz)_3](NO_3)_2$ compound exhibits a spin transition with a thermal hysteresis loop, characterized by the thermal dependence of its $\chi_M T$ product (Figure 1a), where χ_M is the molar magnetic susceptibility and T is the temperature. $\chi_M T$ directly relates to the SCO parameter q, through the weighted contribution of the number N_{HS} of paramagnetic HS sites (χ_M^{HS} with $S = 2$) and N_{LS} of diamagnetic LS sites (χ_M^{LS} with $S = 0$). At room temperature, the $\chi_M T$ value is close to 0, consistent with a fully LS (S = 0) state. Upon warming, the increase of $\chi_M T$ around $T_{\uparrow}$= 346 K corresponds to a thermal conversion toward the higher entropy HS phase. A thermal hysteresis appears upon cooling and the thermal conversion toward the LS state occurs around $T_{\downarrow}$ = 318 K, which corresponds to a thermal hysteresis width $\Delta T \approx 28$ K. These magnetic SCO features are fully consistent with those previously reported for this compound,[38,41] and the $\chi_M T$ curve can be scaled according to the SCO parameter from $q = -1$ to $q = 1$ (Figure 1a). As it is the case for other trz-based SCO materials, this spin transition is accompanied by a pronounced and reversible color change from pink in the LS state to white in the HS state (Figure 1a). Therefore, we also measured variable-temperature UV−vis absorption spectroscopy to monitor the thermally induced spin transition. Figure 1b shows the optical absorption spectra recorded upon cooling and heating between 290 and 360 K. There is a clear evolution of the d−d absorption bands, centered around 530 nm in the LS state, which decays upon heating with the conversion toward the HS state until it vanishes above 340 K. Simultaneously, another absorption band emerges around 800 nm, which is associated with the d-d transition of the HS state. The spectral shift of the d-d band during SCO is associated with the decrease of the ligand field in the HS state. The reverse process occurs upon cooling, and the temperature ranges over which these spectral changes occur are fully

https://doi.org/10.1021/acs.inorgchem.6c02968
Inorg. Chem. 2026, 65, 19485−19494

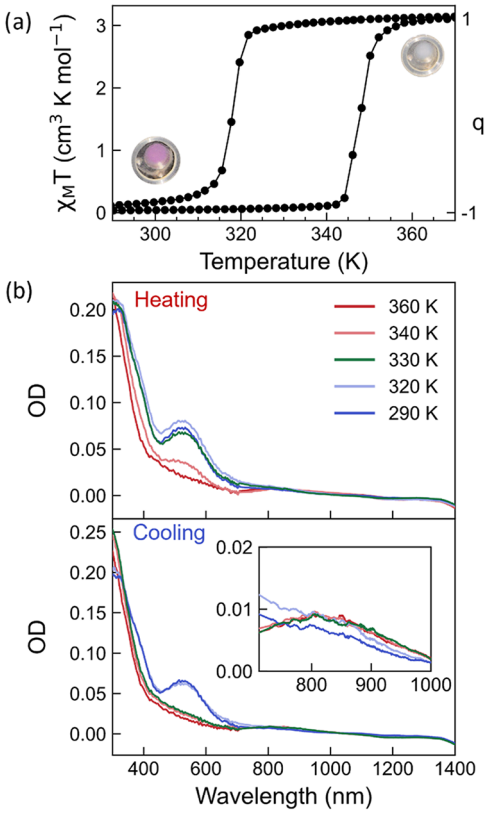

Figure 1. (a) Temperature dependence of the $\chi_M T$ product measured for $[Fe(NH_2trz)_3](NO_3)_2$ during cooling and heating and scaled in the q SCO parameter (right axis), highlighting the strong thermochromism of the material upon the spin transition. The transition temperatures are $T_\uparrow$ = 346 K and $T_\downarrow$ = 318 K, yielding a thermal hysteresis width of ΔT = 28 K. (b) Optical density (OD) spectra recorded upon heating (top) and cooling (bottom). The hysteretic spin transition is characterized by the shift of the *d-d* band, centered around 530 nm for the LS phase to 800 nm for the HS phase (inset).

consistent with the transition temperatures recorded from the magnetic susceptibility data. Both the magnetic and the spectroscopic data constitute a direct fingerprint of the hysteretic spin-transition for the $[Fe(NH_2trz)_3](NO_3)_2$ compound.

The SCO phenomenon is well-known to be associated with important structural reorganizations which can vary greatly from one compound to another, but which are invariably accompanied by an elongation of the metal−ligand bond lengths in the HS state compared to the LS state.[42] The associated reversible volume change related to the SCO typically represents ≈23% of the iron coordination polyhedron.[27] This intramolecular volume modification propagates then across all the physical scales of the material (crystalline lattice, nano-, micro- and macro-metric) within a range of approximately +10% to −15%.[43]

The lattice parameters of the low-temperature LS phase and of the high-temperature HS phase of $[Fe(NH_2trz)_3](NO_3)_2$, obtained from Rietveld refinements, are shown in Table 1. Figure 2 shows the crystalline packing of the $[Fe(NH_2trz)_3]_n$ chains for both phases, projected along the chain axis $\vec{c}$. The lattice periodicity and the symmetry operators are different in the LS and HS phases. The LS lattice is trigonal ($P\bar{3}$) and the unit cell is built from three $[Fe(NH_2trz)_3]_n$ chains. By

Table 1. Unit Cell Structural Parameters of the Low-Temperature LS Phase and of the High-Temperature HS Phase Obtained by Powder X-ray Diffraction at the CRISTAL Beamline of the Synchrotron SOLEIL

	LS	HS
temperature (K)	300	370
chemical formula	$FeN_{14}C_6H_{12}O_6$	$FeN_{14}C_6H_{12}O_6$
crystal system	trigonal	triclinic
space group	$P\bar{3}$	$P\bar{1}$
a(Å)	18.9818(3)	11.8941(15)
b(Å)	18.9818(3)	10.8133(10)
c(Å)	7.31306(11)	7.8339(6)
α (°)	90	81.951(7)
β (°)	90	121.334(7)
γ (°)	120	121.334(7)
Z Fe sites	6	2
volume (Å^3)	2281.94(9)	800.21(13)
R_{wp}	4.184	4.087
R_{exp}	1.763	1.792
GoF/χ2	2.373	2.281

symmetry, the chain located at the origin contains two crystallographically independent Fe(II) sites (Fe_1 and Fe_2) located on the roto-inversion $\bar{3}$ axis. The two other chains are symmetry equivalent and are based on two additional crystallographically independent sites (Fe_3 and Fe_4) lying on a 3-fold axis. Within the unit cell volume (V = 2281.9 Å^3) there are 6 active Fe(II) SCO sites per unit cell. Contrarily, the HS lattice (V = 800.2 Å^3) adopted a triclinic space group $P\bar{1}$. In this case, a unique $[Fe(NH_2trz)_3]_n$ chain can be detected, which is characterized with two independent sites (Fe_1 and Fe_2), lying both on inversion symmetry centers. Considering the unit-cell tripling in the LS with respect to the HS phase, the relative unit-cell volume expansion per chain is $\frac{\Delta V}{V} \approx 5\%$.

Competing Symmetry-Breakings Phenomena

The structural analysis reveals a complex structural reorganization of the chains during the spin transition, with two distinct types of symmetry changes. During the LS to the HS phase transition upon warming, there is a ferroelastic distortion from the trigonal lattice $P\bar{3}$ to the triclinic lattice $P\bar{1}$, due to the loss of the 3-fold symmetry. Ferroelastic transitions are often reported in SCO materials. These reversible phase transitions are associated with a symmetry decrease from a high-symmetry paraelastic phase to a low-symmetry ferroelastic phase, where a spontaneous strain appears.[44] For example, this is the case for the prototype $[Fe(ptz)_6](BF_4)_2$ material,[45−48] which exhibits a ferroelastic transition from the HS $R\bar{3}$ to the LS low-symmetry $P\bar{1}$ phase at ambient pressure as well as a sequential ferroelastic transition $R\bar{3} \rightarrow P\bar{1}$ followed by an SCO transition upon further cooling at high pressure.[35] In case of $[Fe(NH_2trz)_3](NO_3)_2$ studied here, the ferroelastic strain occurs upon warming, which is unusual. Figure 2 shows that in the HS phase the $\vec{c}$ axis is no longer orthogonal to the $(\vec{A},\vec{B})$ plane, due to the loss of 3-fold symmetry, which results in a ferroelastic shear strain and the relative sliding of the chains. This structural instability occurs at the Γ point of the Brillouin zone. On the other hand, there is a decrease in lattice periodicity during the HS to LS phase transition upon cooling. All the $[Fe(NH_2trz)_3]_n$ chains, pointing along the $\vec{c}$ axis, are equivalent by translation symmetry along $\vec{A}$ and $\vec{B}$ in the HS $P\bar{1}$ lattice. In the LS $P\bar{3}$ lattice, there are two types of $[Fe(NH_2trz)_3]_n$ chains

https://doi.org/10.1021/acs.inorgchem.6c02968
Inorg. Chem. 2026, 65, 19485−19494

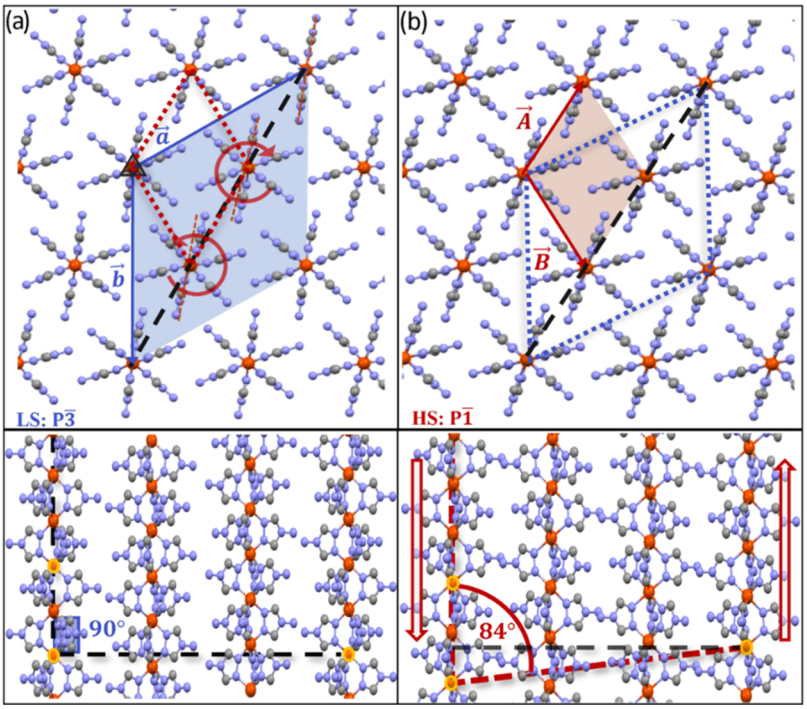

Figure 2. Crystalline packing of the $[Fe(NH_2trz)_3]_n$ chains, projected along and perpendicular to their $\vec{c}$ axis. (a) For the LS $P\bar{3}$ lattice ($\vec{a}$, $\vec{b}$, $\vec{c}$). (b) For the HS $P\bar{1}$ lattice ($\vec{A}$, $\vec{B}$, $\vec{c}$). The loss of the 3-fold symmetry axis in the HS phase results in a ferroelastic shear strain associated with the relative sliding of the chains along the $\vec{c}$ axis (bottom). The rotation of the chains in the LS phase changes the lattice periodicity: the HS unit cell contains one chain, while the LS one contains 3 chains: one at the origin on the $\bar{3}$ Wyckoff position and two equivalent on the 3 Wyckoff positions.

due to their relative rotation (Figure 2). The translation lattice vectors $\vec{A}$ and $\vec{B}$ of the HS phase are lost in the LS phase and this structural instability occurs at the K point $\left(\frac{1}{3}, \frac{1}{3}, 0\right)$ of the Brillouin zone, which is associated with a tripling of the unit-cell volume.

With these two competing changes of symmetry, there is no group-subgroup relationship between the LS and HS phases: the 3-fold symmetry is only present in the LS phase, while the translation symmetry operators $\vec{A}$ and $\vec{B}$ are only present in the HS phase. Consequently, this phase transition does not correspond to a symmetry-breaking. This raises the question of whether this process corresponds to a reconstructive phase transition[49] or a more complex phenomenon. Hereafter, we show that this apparent reconstructive transition is in fact associated with two coupled symmetry-breaking order parameters, deviating from a common parent phase.

A deeper analysis of the structural rearrangements of the $[Fe(NH_2trz)_3]_n$ chains (Figure 2) shows the structural relationships between the lattices of each phase. The LS lattice is defined by the direct vectors $\vec{a},\vec{b},\vec{c}$ (reciprocal vectors $\vec{a}^*,\vec{b}^*,\vec{c}^*$) and the HS lattice by the direct vectors $\vec{A},\vec{B},\vec{c}$ (reciprocal vectors $\vec{A}^*,\vec{B}^*,\vec{c}^*$), with the axis of the $[Fe(NH_2trz)_3]_n$ chains $\vec{c}$ is common to both phases. The lattice vectors of both phases are related by $\vec{a} = 2\vec{A} + \vec{B}$ and $\vec{b} = -\vec{A} + \vec{B}$ and the transformation matrix connecting the HT and LT lattices is $\begin{vmatrix} 2 & -1 & 0 \\ 1 & 1 & 0 \\ 0 & 0 & 1 \end{vmatrix}$. The X-ray scattering vector $\vec{Q}$ of the Bragg peaks can therefore be expressed in both lattices

$$\vec{Q} = h\vec{a}^* + k\vec{b}^* + l\vec{c}^* = H\vec{A}^* + K\vec{B}^* + Lc^*$$

where (hkl) and (HKL) denote the Miller indices of Bragg peaks indexed in the LS and HS reciprocal lattices, respectively. The fundamental orthogonality relationships between the direct and reciprocal lattice vectors relate the Miller indices of the LS and HS phases

$$H = \frac{h-k}{3},\ K = \frac{h+2k}{3},\ L = l$$

In the LS phase, all Bragg peaks indexed with h, k and l integers are allowed, but some of them are not allowed in the HS lattice. For example, Figure 3a shows that the (hkl) Bragg peaks indexed (2 0 0) and (1 0 − 1) are present in the LS phase. These peaks are indexed $H = \frac{2}{3}$, $K = \frac{2}{3}$, $L = 0$ and $H = \frac{1}{3}$, $K = \frac{1}{3}$, $L = -1$ in the HS lattice, where they are not allowed as H and K indices are not integer. These superstructure Bragg peaks of the LS lattice are associated with the tripling of the unit cell volume and appear at the K point $\left(\frac{1}{3}, \frac{1}{3}, 0\right)$ of the Brillouin zone. The amplitude of this symmetry-breaking can be monitored through the order parameter ξ, which probes the difference in the LS phase between the chains that are symmetry-equivalent in the HS phase. The evolution of the intensity of these superstructure Bragg peaks (Figure 3), scaling as ξ^2, represents a direct fingerprint of the unit cell volume tripling between the HS phase with a single chain ($\xi = 0$) and the LS phase with 3 chains per unit cell ($\xi \neq 0$).

Figure 4a shows that, due to the 3-fold symmetry in the reciprocal lattice of the LS phase, the scattering vectors $\vec{Q}$ corresponding to the Bragg peaks indexed (110), (2$\bar{1}$0) and (1$\bar{2}$0), as well as their equivalent by inversion symmetry, have the same modulus. These Bragg peaks correspond to the same diffraction ring around $Q = 0.65$ Å^{-1} (Figure 3a). This is no longer the case for the reciprocal lattice of the HS $P\bar{1}$ lattice

https://doi.org/10.1021/acs.inorgchem.6c02968
Inorg. Chem. 2026, 65, 19485−19494

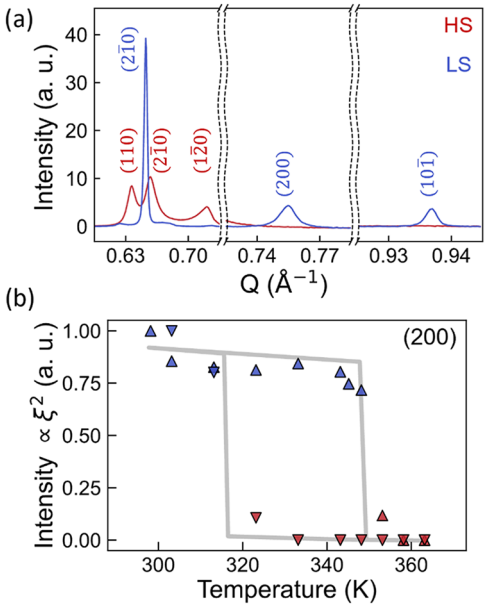

Figure 3. (a) Selected region of the powder X-ray diffraction patterns for the LS phase (blue) and HS phase (red). Upon heating, the Bragg peaks indexed (200) and (10$\bar{1}$) in the LS lattice disappear in the HS phase due to the change of lattice periodicity, while the peak (2$\bar{1}$0) splits into the (2$\bar{1}$0), (1$\bar{2}$0) and (110) Bragg peaks due to the ferroelastic distortion. (b) The thermal dependence of the intensity of the (200) peak shows that the change of lattice periodicity follows the SCO thermal hysteresis, shown as an eye guide based on Figure 1a.

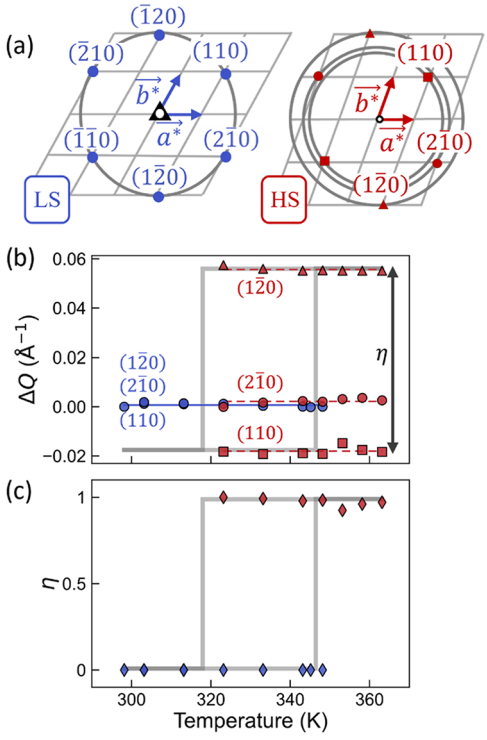

Figure 4. (a) Representation of the reciprocal lattice in the ($\vec{a}$*,$\vec{b}$*) plane for the LS $P\bar{3}$ and distorted HS $P\bar{1}$ phases. In the LT phase, the six nodes of the reciprocal lattice shown have the same Q modulus and lie on the same diffraction ring. In the ferroelastic HT phase, the nodes lie on three distinct rings indicated by different symbols corresponding to three scattering vectors Q. (b) Shift with temperature of the scattering vector Q modulus with respect to the LS phase, for the (110), (2$\bar{1}$0) and (1$\bar{2}$0) Bragg peaks. (c) Thermal dependence of the normalized magnitude of the splitting along Q, proportional to the ferroelastic distortion order parameter η. The hysteresis shown is a guide to the eye based on the transition temperatures from Figure 1a.

(Figure 4a). Due to the ferroelastic distortion, these Bragg peaks correspond to 3 different diffraction rings, as observed in the powder X-ray diffraction data (Figure 3a) around Q = 0.64 Å^{-1} for (110), Q = 0.66 Å^{-1} for (2$\bar{1}$0) and Q = 0.72 Å^{-1} for (1$\bar{2}$0). Figure 4b shows that upon warming, the single Bragg peak in the LS phase splits in 3 around $T_{\uparrow}$= 346 K in the HS phase. The splitting ΔQ of these Bragg peaks is related to the ferroelastic order parameter η and it monitors the deviation of the HS $P\bar{1}$ lattice from the LS $P\bar{3}$ lattice. The ferroelastic strain, related to the relative splitting of the Bragg peaks, is quite large ($\frac{\Delta Q}{Q} \approx 11\%$). Upon cooling, the three Bragg peaks merge into a single peak around $T_{\downarrow}$ = 318 K. Figure 4c shows the thermal dependence of the amplitude of the ferroelastic distortion η, scaled to 1 for clarity, which follows the same thermal hysteresis as the spin transition curve (Figure 1a).

Figure 5 shows that the LS to HS transition is associated with an increase in all the lattice parameters a, b and c (common to both phases), following a classical positive thermal expansion, which is not always the case in SCO materials.[50] The evolution of the chain axis c between the LS and HS phases is consistent with the one reported for the [Fe(Htrz)$_2$(trz)](BF$_4$) complex (~7.3 Å in LS and ~7.8 Å in HS).[51] It is a direct marker of the spin transition in the [Fe(R-trz)$_3$]X$_2$ materials associated with the evolution of the Fe-ligand distances within the polymeric chains. In the LS $P\bar{3}$ phase, a and b are symmetry equivalent (by definition), while their splitting in the HS $P\bar{1}$ phase is the signature of the ferroelastic distortion.

Overall, these considerations on the structural changes in the packing of the [Fe(NH$_2$trz)$_3$]$_n$ chains during the spin transition reveal that the material exhibits a hysteretic spin state conversion (Figure 1) coupled to symmetry changes (Figure 2), but with no group-subgroup relationship between the LS and HS phases. Upon heating, the LS to HS phase transition involves a concomitant ferroelastic distortion (loss of 3-fold symmetry, Figure 4) and gain of some translational symmetry (Figure 3), while upon cooling the HS to LS transition involves the concomitant gain of 3-fold symmetry and loss of some translational symmetry. Consequently, this structural phase transition cannot be described by the usual Landau theory, through the evolution of a single order parameter. Two order parameters are then required for monitoring the ferroelastic distortion (η) with the loss of 3-fold symmetry and the loss of translation symmetry (ξ).

Theoretical Phase Diagram Determination

The theory of phase transitions described by two symmetry-breaking order parameters was discussed in the literature for diverse types of materials.[49,52−56] The two order parameters evolve simultaneously during the phase transition and are coupled. A symmetry analysis shows that in the present case both the LT and HT phases can be described as low symmetry phases of a common higher symmetry parent phase, called hereafter phase 0. Figure 6a schematically shows phase 0, which corresponds to a $P\bar{3}$ lattice with the periodicity of the HS phase, i.e. with a single [Fe(NH$_2$trz)$_3$]$_n$ chain per unit cell. This high-symmetry phase 0, corresponding to η = 0 and ξ = 0, is not observed in these measurements. This symmetry analysis

https://doi.org/10.1021/acs.inorgchem.6c02968
Inorg. Chem. 2026, 65, 19485−19494

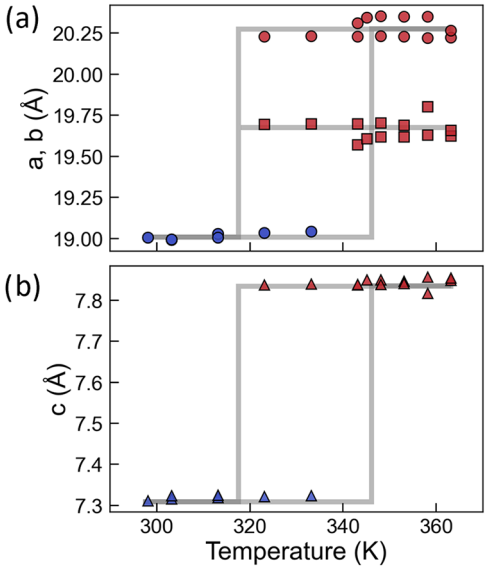

Figure 5. Thermal dependence of the lattice parameters common to both phases. (a) *a* (circles) and *b* (squares) axes are symmetry equivalent in the LS $P\bar{3}$ phase and differ in the HS $P\bar{1}$ phase. (b) The parameter *c* (triangles) is a direct marker of the spin transition in the $[Fe(NH_2trz)_3]_n$ chain. The hysteresis shown is a guide to the eye based on the transition temperatures from Figure 1a.

was confirmed by using the ISOTROPY software suite and the Bilbao Crystallographic Server tools.[57,58] In this way, the high spin triclinic HT Phase I corresponds to $\eta \neq 0$ and $\xi = 0$. It has the same lattice periodicity as the parent phase, with a single $[Fe(NH_2trz)_3]_n$ chain per unit cell, but with a distorted $P\bar{1}$ lattice with respect to phase 0. The order-parameter space corresponding to η is associated with the two-dimensional irreducible representation k16t3t5 (Kovalev' notation) of phase 0. The low spin rhombohedral LT phase II corresponds to $\eta = 0$, $\xi \neq 0$. It has the same $P\bar{3}$ lattice symmetry as the parent phase, but the cell multiplicity results in different $[Fe(NH_2trz)_3]_n$ chains within the unit cell with respect to phase 0. The order-parameter space corresponding to ξ is associated with the one-dimensional irreducible representation k13t1 of phase 0. Based on the calculation of invariants associated with the symmetry-breaking parameters, we express the Landau development of the Gibbs potential *G* as

$$G(\eta, \xi) = \alpha_1\eta^2 + b_1\eta^3 + c_1\eta^4 + \alpha_2\xi^2 + b_2\xi^3 + c_2\xi^4 + D\eta^2\xi^2 \quad (1)$$

The $\alpha_2\xi^2 + b_2\xi^3 + c_2\xi^4$ terms are the cell multiplicity invariant polynomials. This potential corresponds to a discontinuous (first-order) transition when a cubic term is present and a continuous (second-order) transitions when the quartic term is positive and the cubic term vanishes ($b_2 = 0$).[59] In order to limit the number of parameters in the theoretical potential, the choice is made to consider the second-order case, which allows distinguishing more easily both transitions. The $\alpha_1\eta^2 + b_1\eta^3 + c_1\eta^4$ terms correspond to the usual Landau potential for the ferroelastic $P_{\bar{3}}$ to $P_{\bar{1}}$ transition associated with the loss of 3-fold symmetry,[44,60−62] which is restricted to be discontinuous. This is a simplified form in which the two-component order parameter η is reduced to a single component for the sake of presentation. This point was discussed in the similar case of the RbMnFe material, exhibiting cubic-tetragonal ferroelastic distortion associated with the loss of 3-fold symmetry.[37] The $D\eta^2\xi^2$ term is the lowest-order coupling term allowed.[56] $D > 0$ corresponds to the competing symmetry-breaking phenomena observed here. α_1 and α_2 are the reduced temperatures, with $\alpha_1 = a_1(T - T_\eta)$ and $\alpha_2 = a_2(T - T_\xi)$, where T_η and T_ξ are the critical temperatures for each symmetry-breaking process. The b_i and c_i coefficients are considered as constants. This model can describe a complex phase diagram, where four phases can emerge. Finally, phase III corresponds to the lowest symmetry phase ($\eta \neq 0$, $\xi \neq 0$), with a tripled cell multiplicity and a ferroelastic distortion, which is not observed in these measurements. Previous works discussed the biquadratic coupling between two order parameters, where one exhibits

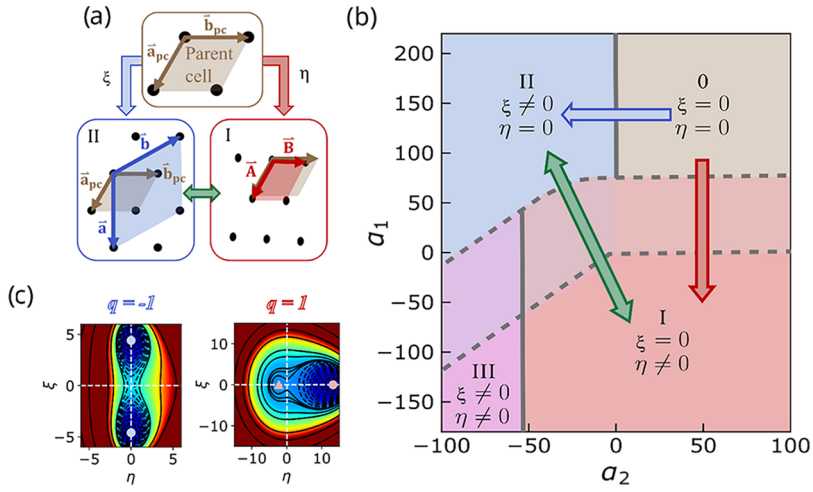

Figure 6. (a) Schematic relationships between the HS phase I and the LS phase II. The lattice periodicity of the parent cell corresponding to phase 0 is defined by the parameters $\vec{a}_{pc}$, $\vec{b}_{pc}$, *and it exhibits* $P\bar{3}$ *symmetry* ($a_{pc} = b_{pc}$, $\gamma = 120°$). *The ferroelastic distortion* (η) *leads to phase I* ($P\bar{1}$) *with a lattice* $\vec{A}$, $\vec{B}$, $\vec{c}$ *distorted compared to phase 0. The superlattice ordering of the chains* (ξ) *leads to phase II. (b) Calculated phase diagram from eq (1). The solid lines denote second-order superlattice transitions (blue arrow) and dotted lines represent stability limits of the hysteresis during the ferroelastic transition (red arrow). The green arrows show the transition from the LS phase (II) to the HS phase (I). (c) Calculated potential showing the equilibrium LS tripled cell* ($q = -1$, $\xi \neq 0$, $\eta = 0$) *and HS ferroelastic* ($q = 1$, $\xi = 0$, $\eta \neq 0$) *phases.*

https://doi.org/10.1021/acs.inorgchem.6c02968
Inorg. Chem. 2026, 65, 19485−19494

a discontinuous transition, through a η^2, η^4, η^6 potential.[49,52,55] However, in our case, we have to use and η^2, η^3, η^4 potential due to symmetry consideration.[60,63] Since this potential has no analytical solution, we performed a numerical study of the potential, identifying and classifying the thermal evolution of the minima in the potential calculated for different values of η and ξ. For the calculation, we used $\alpha_1 = 1$, $b_1 = 50/3$, $c_1 = 5/4$, $= 1/2$, $c_2 = 5/4$, $D = 3$, which were chosen to qualitatively reproduce the experimental phase sequence. While no quantitative fitting to experimental data was attempted, the topology of the calculated phase diagram, and in particular the existence of a direct transition between the ferroelastic phase I and the superlattice phase II, is governed by the sign and the relative magnitude of the coefficients and the coupling constant $D > 0$, rather than by the specific values of the individual coefficients.

Figure 6b shows the calculated phase diagram, with a hysteretic phase transition from the parent phase 0 to the ferroelastic phase I (corresponding to the symmetry of the HS phase), and a continuous phase transition from phase 0 to phase II (corresponding to the symmetry of the LS phase with tripled unit cell). More interestingly, the calculated diagram reveals a hysteretic phase transition from phase I to phase II. This phase transition line, indicated by the green arrow, corresponds to the symmetry change observed between the HS phase (triclinic: $\eta \neq 0$ and single chain $\xi = 0$) and the LS phase (rhombohedral: $\eta = 0$ and cell tripling $\xi \neq 0$), which is observed experimentally. However, this Landau theory-based model and the associated phase diagram does not consider the spin transition parameter q, which is known to be the driving force of the thermal transition, due to the important entropy increase in the HS state.[18,34,36]

Recent studies have shown the importance of considering the effect of the coupling between the SCO parameter q and the symmetry-breaking in the Landau development of the thermodynamical potential.[22,33−36] In the present case, the Landau development considering the different symmetry-breaking processes, the SCO, and their coupling, leads to a complex potential

$$G(q,\eta,\xi) = aq + \frac{b}{2}q^2 + \frac{c}{4}q^4 + \alpha_1\eta^2 + b_1\eta^3 + c_1\eta^4 + \alpha_2\xi^2 + b_2\xi^4 + D\eta^2\xi^2 + Eq\eta^2 + Fq\xi^2 \quad (2)$$

where the q, q^2, q^4 terms correspond to the SCO potential introduced by Chernysov et al. to describe isosymmetric and stepwise spin transitions,[21] where a is the reduced SCO temperature. The $Eq\eta^2$ and + $Fq\xi^2$ terms correspond to the coupling of the SCO parameter with the ferroelastic and superlattice symmetry-breakings, as introduced by Collet to describe SCO coupled to various symmetry breaking phenomena.[35−37] Here we consider $E < 0$ that favors a HS ferroelastic phase ($q = 1$, $\eta \neq 0$,$\xi = 0$) and $F > 0$ that favors a LS superlattice phase ($q = -1$, $\eta = 0$, $\xi \neq 0$). In the strong coupling limit,[34] where the different processes are mainly driven by the SCO process ($\alpha_1\eta^2 \ll Eq\eta^2$ and $\alpha_2\xi^2 \ll Fq\xi^2$), the potential can be simplified to

$$G(q,\eta,\xi) = aq + \frac{b}{2}q^2 + \frac{c}{4}q^4 + b_1\eta^3 + c_1\eta^4 + b_2\xi^4 + D\eta^2\xi^2 + Eq\eta^2 + Fq\xi^2 \quad (3)$$

This limit is justified by the experimental observation that both the ferroelastic distortion parameter η (Figure 4c) and the unit cell tripling parameter ξ (Figure 3b) follow the same thermal hysteresis as the spin transition parameter q (Figure 1a). This indicates that the entropy-driven thermal evolution of the SCO parameter q is the primary parameter driving, through the $Eq\eta^2$ and $Fq\xi^2$ couplings, both symmetry-breaking phenomena. Defining the equilibrium conditions for the 3 order parameters is complex. However, it was recently shown that strong couplings of SCO to symmetry-breaking parameters stabilize a sample[34] in the sense that all its Fe atoms adopt the same spin state, i.e LS ($q = -1$) or HS states ($q = 1$), as observed here. Then, we can investigate the equilibrium condition of the symmetry-breaking potential G_{SB} in the (η,ξ) space.

In the LS phase where $q = -1$: $G_{SB}(\eta,\xi) = -E\eta^2 + b_1\eta^3 + c_1\eta^4 - F\xi^2 + b_2\xi^4 + D\eta^2\xi^2$

In the HS phase where $q = +1$: $G_{SB}(\eta,\xi) = +E\eta^2 + b_1\eta^3 + c_1\eta^4 + F\xi^2 + c_2\xi^4 + D\eta^2\xi^2$

The equilibrium (η,ξ) values are found by numerically minimizing the potentials for the LS and HS phases. We used $E = -2$ and $F = 2$ to calculate the symmetry-breaking potential $G_{SB}(\eta,\xi)$ in Figure 6c. For the HS phase ($q = 1$), the equilibrium is found for $\xi = 0$ and $\eta \neq 0$, which corresponds to the ferroelastic phase I. For the LS phase ($q = -1$) the equilibrium is found for $\xi \neq 0$ and $\eta = 0$, which corresponds to the LS supercell phase II. The complex phase transition of the $[Fe(NH_2trz)_3](NO_3)_2$ compound can therefore be rationalized as resulting from the coupling of the SCO to two competing symmetry-breaking phenomena: the ferroelastic lattice distortion and the unit-cell tripling. We can notice that including the ξ^3 term ($b_2 \neq 0$) in the eq (3) for the cell tripling transition would not change the main conclusion of our study: the 0-I phase transition that is not observed here would be discontinuous, while the phase transition from the HT phase I to the LT phase II would still be discontinuous.

CONCLUSIONS

Our results show a very complex phase transition in the SCO material $[Fe(NH_2trz)_3](NO_3)_2$, where a ferroelastic strain occurs upon heating toward the HS phase, and a unit cell tripling occurs upon cooling toward the LS phase. To our knowledge, such a competition between two competing symmetry-breaking phenomena, coupled to a spin transition, has not been reported so far and it can only result in a hysteretic behavior. This opens the way for a complex phase diagram, where HS and LS bistability compete with various types of symmetry-breaking and structural ordering. In the present case, we show that the emergence of a thermal hysteresis associated with the spin state conversion results from the coupling of the SCO parameter with both competing symmetry-breaking phenomena.

AUTHOR INFORMATION

Corresponding Authors

Laurent Guérin − *Univ Rennes, CNRS, IPR (Institut de Physique de Rennes) - UMR 6251, 35000 Rennes, France; CNRS, Univ Rennes, DYNACOM (Dynamical Control of Materials Laboratory) - IRL 2015, The University of Tokyo, Tokyo 113-0033, Japan;* orcid.org/0000-0002-0509-8444; Email: laurent.guerin@univ-rennes.fr

https://doi.org/10.1021/acs.inorgchem.6c02968
Inorg. Chem. 2026, 65, 19485−19494

Eric Collet − *Univ Rennes, CNRS, IPR (Institut de Physique de Rennes) - UMR 6251, 35000 Rennes, France; CNRS, Univ Rennes, DYNACOM (Dynamical Control of Materials Laboratory) - IRL 2015, The University of Tokyo, Tokyo 113-0033, Japan; Institut Universitaire de France (IUF), 75000 Paris, France;* orcid.org/0000-0003-0810-7411; Email: eric.collet@univ-rennes.fr

Authors

Maryam Alashoor − *Univ Rennes, CNRS, IPR (Institut de Physique de Rennes) - UMR 6251, 35000 Rennes, France; CNRS, Univ Rennes, DYNACOM (Dynamical Control of Materials Laboratory) - IRL 2015, The University of Tokyo, Tokyo 113-0033, Japan*

Ricardo G. Torres Ramírez − *Univ Rennes, CNRS, IPR (Institut de Physique de Rennes) - UMR 6251, 35000 Rennes, France*

Olaf Stefanczyk − *CNRS, Univ Rennes, DYNACOM (Dynamical Control of Materials Laboratory) - IRL 2015, The University of Tokyo, Tokyo 113-0033, Japan; Department of Chemistry, School of Science, The University of Tokyo, Tokyo 113-0033, Japan;* orcid.org/0000-0003-0955-5646

Kazuki Nakamura − *Univ Rennes, CNRS, IPR (Institut de Physique de Rennes) - UMR 6251, 35000 Rennes, France; CNRS, Univ Rennes, DYNACOM (Dynamical Control of Materials Laboratory) - IRL 2015, The University of Tokyo, Tokyo 113-0033, Japan;* orcid.org/0009-0009-3807-3567

Francisco Javier Valverde-Muñoz − *Univ Rennes, CNRS, IPR (Institut de Physique de Rennes) - UMR 6251, 35000 Rennes, France;* orcid.org/0000-0003-3578-5445

Elzbieta Trzop − *Univ Rennes, CNRS, IPR (Institut de Physique de Rennes) - UMR 6251, 35000 Rennes, France; CNRS, Univ Rennes, DYNACOM (Dynamical Control of Materials Laboratory) - IRL 2015, The University of Tokyo, Tokyo 113-0033, Japan*

Ivan da Silva − *ISIS Neutron and Muon Source, Rutherford Appleton Laboratory, OX11 0QX Didcot, United Kingdom;* orcid.org/0000-0002-4472-9675

Shin-ichi Ohkoshi − *CNRS, Univ Rennes, DYNACOM (Dynamical Control of Materials Laboratory) - IRL 2015, The University of Tokyo, Tokyo 113-0033, Japan; Department of Chemistry, School of Science, The University of Tokyo, Tokyo 113-0033, Japan;* orcid.org/0000-0001-9359-5928

Arnaud Grosjean − *Univ. Bordeaux, CNRS, Bordeaux INP, ICMCB, UMR5026, 33600 Pessac, France; National Synchrotron Radiation Research Center, Hsinchu 30092, Taiwan*

Nathalie Daro − *Univ. Bordeaux, CNRS, Bordeaux INP, ICMCB, UMR5026, 33600 Pessac, France*

Philippe Guionneau − *Univ. Bordeaux, CNRS, Bordeaux INP, ICMCB, UMR5026, 33600 Pessac, France*

Complete contact information is available at: https://pubs.acs.org/10.1021/acs.inorgchem.6c02968

Author Contributions

Conceptualization: E.C, L.G. methodology: E.C., L.G., M.A., R.G.T.R., I.S., E.T., F.J.V.M., K.N. and O.S. synthesis and characterization: A.G., N.D. and P.G. investigation: E.C., L.G., M.A., R.G.T.R., E.T., F.J.V.M., N.D., P.G. resources: E.C., L.G., S.O., N.D. and P.G. formal analysis: E.C., L.G., M.A., R.G.T.R., E.T., A.G., N.D. and P.G. funding acquisition: E.C., L.G., S.O. and P.G. project administration: E.C., L.G. supervision: E.C., L.G. writing—original draft: E.C., L.G., M.A. writing—review and editing: E.C., L.G., M.A., R.G.T.R., O.S., K.N., F.J.V.M., E.T., I.S., S.O., A.G., N.D., P.G.

Funding

Agence Nationale de la Recherche (grant ANR-19-CE30−0004 ELECTROPHONE). Joint PhD Programme call University of Tokyo and CNRS. JSPS KAKENHI (Grant Number 25H00866), the Advanced Technologies for Carbon-Neutral (ALCA-Next) from JST (JPMJAN23A2), IRL DYNACOM (CNRS), the CNRS-University of Tokyo "Excellence Science" Joint Research Program, and the Second CNRS-University of Tokyo PhD Joint Program, and the MEXT Quantum Leap Flagship Program (JPMXS0118068681) for the support.

Notes

The authors declare no competing financial interest.

■ ACKNOWLEDGMENTS

E.C. thanks the University Rennes and the Fondation Rennes 1 for funding. The authors thank Région Bretagne, Ille-Et-Vilaine Department, French Ministry of Research, R.M., CNRS, European Union for financial support (CPER Project Mat&Trans 2021-2027). This work was partially supported by a Grant-in-Aid for Scientific Research (A) from JSPS KAKENHI (Grant Number 25H00866), the Advanced Technologies for Carbon-Neutral (ALCA-Next) from JST (JPMJAN23A2), IRL DYNACOM (CNRS), the CNRS-University of Tokyo "Excellence Science" Joint Research Program, and the Second CNRS-University of Tokyo PhD Joint Program. The authors acknowledge the Cryogenic Research Center (University of Tokyo), the Center for Nano Lithography & Analysis (University of Tokyo) supported by MEXT, and the MEXT Quantum Leap Flagship Program (JPMXS0118068681) for the support. This project has received funding from the European Union's Horizon 2020 research and innovation program under the Marie Sklodowska-Curie grant agreement No 899546 (MSCA-COFUND BIENVENÜE). The authors gratefully acknowledge the support of Erik Elkaim and El-Eulmi Bendeif during the synchrotron experiment carried out at the CRISTAL beamline of the French national synchrotron facility SOLEIL.

■ REFERENCES

(1) Halcrow, M. A. *Spin-Crossover Materials: Properties and Applications*; John Wiley & Sons, Ltd: Chichester, 2013; p 546.

(2) Molnár, G.; Mikolasek, M.; Ridier, K.; Fahs, A.; Nicolazzi, W.; Bousseksou, A. Molecular Spin Crossover Materials: Review of the Lattice Dynamical Properties. *Ann. Phys-Berlin* **2019**, *531* (10), No. 1900076.

(3) Gütlich, P.; Goodwin, H. A. Spin crossover - An overall perspective. *Spin Crossover Trans. Metal Compd. I* **2004**, *233*, 1−47.

(4) Kahn, O.; Martinez, C. J. Spin-transition polymers: From molecular materials toward memory devices. *Science* **1998**, *279* (5347), 44−48.

(5) Enriquez-Cabrera, A.; Rapakousiou, A.; Bello, M. P.; Molnár, G.; Salmon, L.; Bousseksou, A. Spin crossover polymer composites, polymers and related soft materials. *Coord. Chem. Rev.* **2020**, *419*, No. 213396.

(6) Reinhard, M.; Kunnus, K.; Ledbetter, K.; Biasin, E.; Bregenholt Zederkof, D.; Alonso-Mori, R.; Brandt van Driel, T.; Nelson, S.;

Kozina, M.; Borkiewicz, O. J.; Lorenc, M.; Cammarata, M.; Collet, E.; Sokaras, D.; Cordones, A. A.; Gaffney, K. J. Observation of a picosecond light-induced spin transition in polymeric nanorods. *ACS Nano* **2024**, *18*, 15468−15476, DOI: 10.1021/acsnano.3c10042.
(7) Ridier, K.; Bas, A.-C.; Shalabaeva, V.; Nicolazzi, W.; Salmon, L.; Molnár, G.; Bousseksou, A.; Lorenc, M.; Bertoni, R.; Collet, E.; Cailleau, H. Finite Size Effects on the Switching Dynamics of Spin-Crossover Thin Films Photoexcited by a Femtosecond Laser Pulse. *Adv. Mater.* **2019**, *31* (25), No. 1901361.
(8) Tiwari, B.; Trapali, A.; Molnár, G.; Salmon, L.; Bousseksou, A. Design and development of a self-sensing control for spin crossover based soft electrothermal actuators. *Smart Mater. Struct.* **2026**, *35* (1), No. 015043.
(9) Gallé, G.; Deldicque, D.; Degert, J.; Forestier, T.; Létard, J. F.; Freysz, E. Room temperature study of the optical switching of a spin crossover compound inside its thermal hysteresis loop. *Appl. Phys. Lett.* **2010**, *96* (4), No. 041907.
(10) Roubeau, O. Triazole-based one-dimensional spin-crossover coordination polymers. *Chemistry* **2012**, *18* (48), 15230−15244.
(11) Grosjean, A.; Daro, N.; Kauffmann, B.; Kaiba, A.; Letard, J. F.; Guionneau, P. The 1-D polymeric structure of the $[Fe(NH_2trz)_3](NO_3)_2$. nH_2O (with n = 2) spin crossover compound proven by single crystal investigations. *Chem. Commun.* **2011**, *47* (45), 12382−12384.
(12) Kroeber, J.; Audiere, J.-P.; Claude, R.; Codjovi, E.; Kahn, O.; Haasnoot, J. G.; Groliere, F.; Jay, C.; Bousseksou, A. Spin Transitions and Thermal Hysteresis in the Molecular-Based Materials $[Fe(Htrz)_2(trz)](BF_4)$ and $[Fe(Htrz)_3](BF_4)_2.H_2O$ (Htrz = 1,2,4−4H-triazole; trz = 1,2,4-triazolato). *Chem. Mater.* **1994**, *6* (8), 1404−1412.
(13) Yokoyama, T.; Murakami, Y.; Kiguchi, M.; Komatsu, T.; Kojima, N. Spin-crossover phase transition of a chain Fe(II) complex studied by x-ray-absorption fine-structure spectroscopy. *Phys. Rev. B* **1998**, *58* (21), No. 14238.
(14) Verelst, M.; Sommier, L.; Lecante, P.; Mosset, A.; Kahn, O. Structural Study by Wide-Angle X-ray Scattering of the Spin Transition Molecular Materials $[Fe(Htrz)_2(trz)](BF_4)$ and $[Fe(NH_2trz)_3](NO_3)_2$ (Htrz = 1,2,4−4H-Triazole, trz = 1,2,4-Triazolato). *Chem. Mater.* **1998**, *10* (4), 980−985.
(15) Dîrtu, M. M.; Neuhausen, C.; Naik, A. D.; Rotaru, A.; Spinu, L.; Garcia, Y. Insights into the Origin of Cooperative Effects in the Spin Transition of $[Fe(NH_2trz)_3](NO_3)_2$: the Role of Supramolecular Interactions Evidenced in the Crystal Structure of $[Cu(NH_2trz)_3](NO_3)_2{\cdot}H_2O$. *Inorg. Chem.* **2010**, *49* (12), 5723−5736.
(16) Urakawa, A.; Van Beek, W.; Monrabal-Capilla, M.; Galán-Mascarós, J. R.; Palin, L.; Milanesio, M. Combined, Modulation Enhanced X-ray Powder Diffraction and Raman Spectroscopic Study of Structural Transitions in the Spin Crossover Material $[Fe(Htrz)_2(trz)](BF_4)$. *J. Phys. Chem. C* **2011**, *115* (4), 1323−1329.
(17) Michalowicz, A.; Moscovici, J.; Ducourant, B.; Cracco, D.; Kahn, O. EXAFS and X-ray powder diffraction studies of the spin transition molecular materials $[Fe(Htrz)_2(trz)](BF_4)$ and $[Fe(Htrz)_3](BF_4)_2.H_2O$ (Htrz = 1,2,4−4H-triazole; trz = 1,2,4-triazolato). *Chem. Mater.* **1995**, *7* (10), 1833−1842.
(18) Nicolazzi, W.; Bousseksou, A. Thermodynamical aspects of the spin crossover phenomenon. *Cr Chim.* **2018**, *21* (12), 1060−1074.
(19) Dayen, J.-F.; Konstantinov, N.; Palluel, M.; Daro, N.; Kundys, B.; Soliman, M.; Chastanet, G.; Doudin, B. Room temperature optoelectronic devices operating with spin crossover nanoparticles. *Mater. Horiz.* **2021**, *8* (8), 2310−2315.
(20) Piedrahita-Bello, M.; Angulo-Cervera, J. E.; Enriquez-Cabrera, A.; Molnár, G.; Tondu, B.; Salmon, L.; Bousseksou, A. Colossal expansion and fast motion in spin-crossover@polymer actuators. *Mater. Horiz.* **2021**, *8* (11), 3055−3062.
(21) Chernyshov, D.; Bürgi, H.-B.; Hostettler, M.; Törnroos, K. W. Landau theory for spin transition and ordering phenomena in Fe(II) compounds. *Phys. Rev. B* **2004**, *70*, No. 094116.
(22) Azzolina, G.; Bertoni, R.; Collet, E. General Landau theory of non-symmetry-breaking and symmetry-breaking spin transition materials. *J. Appl. Phys.* **2021**, *129* (8), No. 085106.
(23) Kulmaczewski, R.; Trzop, E.; Kershaw Cook, L. J.; Collet, E.; Chastanet, G.; Halcrow, M. A. The role of symmetry breaking in the structural trapping of light-induced excited spin states. *Chem. Commun.* **2017**, *53* (99), 13268−13271.
(24) Shatruk, M.; Phan, H.; Chrisostomo, B. A.; Suleimenova, A. Symmetry-breaking structural phase transitions in spin crossover complexes. *Coord. Chem. Rev.* **2015**, *289*−*290*, 62−73.
(25) Paliwoda, D.; Vendier, L.; Nicolazzi, W.; Molnár, G.; Bousseksou, A. Pressure Tuning of Coupled Structural and Spin State Transitions in the Molecular Complex $[Fe(H2B(pz)_2)_2(phen)]$. *Inorg. Chem.* **2022**, *61* (40), 15991−16002.
(26) Chernyshov, D.; Hostettler, M.; Tornroos, K. W.; Burgi, H. B. Ordering phenomena and phase transitions in a spin-crossover compound-uncovering the nature of the intermediate phase of $[Fe(2\text{-}pic)_3]Cl_2$.EtOH. *Angew. Chem., Int. Ed.* **2003**, *42* (32), 3825−3830.
(27) Wu, Y.; Peng, S.; Zhang, Z.; Gao, Y.; Xu, G.; Dai, J.; Li, Z. Y.; Yamashita, M. Controlling Three-Step and Five-Step Spin Transitions by Polymorphism in an Fe^{III} Spin Crossover Complex. *Chin. J. Chem.* **2024**, *42*, 879−886, DOI: 10.1002/cjoc.202300679.
(28) Jakobsen, V. B.; Trzop, E.; Gavin, L. C.; Dobbelaar, E.; Chikara, S.; Ding, X.; Esien, K.; Müller-Bunz, H.; Felton, S.; Zapf, V. S.; Collet, E.; Carpenter, M. A.; Morgan, G. G. Stress-Induced Domain Wall Motion in a Ferroelastic Mn^{3+} Spin Crossover Complex. *Angew. Chem., Int. Ed.* **2020**, *59* (32), 13305−13312.
(29) Bonnet, S.; Siegler, M. A.; Costa, J. S.; Molnar, G.; Bousseksou, A.; Spek, A. L.; Gamez, P.; Reedijk, J. A two-step spin crossover mononuclear iron(ii) complex with a [HS-LS-LS] intermediate phase. *Chem. Commun.* **2008**, No. 43, 5619−5621.
(30) Ortega-Villar, N.; Muñoz, C. M.; Real, A. J. Symmetry Breaking in Iron(II) Spin-Crossover Molecular Crystals. *Magnetochemistry* **2016**, *2* (1), No. 16.
(31) Craig, G. A.; Costa, J. S.; Roubeau, O.; Teat, S. J.; Aromí, G. Coupled Crystallographic Order−Disorder and Spin State in a Bistable Molecule: Multiple Transition Dynamics. *Chem. - Eur. J.* **2011**, *17* (11), 3120−3127.
(32) Watanabe, H.; Tanaka, K.; Bréfuel, N.; Cailleau, H.; Létard, J.-F.; Ravy, S.; Fertey, P.; Nishino, M.; Miyashita, S.; Collet, E. Ordering phenomena of high-spin/low-spin states in stepwise spin-crossover materials described by the ANNNI model. *Phys. Rev. B* **2016**, *93*, No. 014419.
(33) Ramírez, R. G. T.; Trzop, E.; Collet, E. Magnetoelectric and MIESST effects in spin crossover materials exhibiting symmetry-breaking. *Dalton Trans.* **2024**, *53* (24), 10159−10167.
(34) Valverde-Muñoz, F. J.; Ramirez, R. G. T.; Trzop, E.; Bataille, T.; Daro, N.; Denux, D.; Guionneau, P.; Cailleau, H.; Chastanet, G.; Le Guennic, B.; Collet, E. Stabilizing low symmetry-based functions of materials at room temperature through isosymmetric electronic bistability. *Mater. Horiz.* **2025**, *12* (5), 1463−1472.
(35) Collet, E.; Azzolina, G.; Jeftić, J.; Lemée-Cailleau, M.-H. Coupled spin cross-over and ferroelasticity: revisiting the prototype $[Fe(ptz)_6](BF_4)_2$ material. *Adv. Phys.: X* **2023**, *8* (1), No. 2161936.
(36) Collet, E.; Azzolina, G. Coupling and decoupling of spin crossover and ferroelastic distortion: Unsymmetric hysteresis loop, phase diagram, and sequence of phases. *Phys. Rev. Mater.* **2021**, *5* (4), No. 044401.
(37) Azzolina, G.; Bertoni, R.; Ecolivet, C.; Tokoro, H.; Ohkoshi, S.; Collet, E. Landau theory for non-symmetry-breaking electronic instability coupled to symmetry-breaking order parameter applied to Prussian blue analog. *Phys. Rev. B* **2020**, *102* (13), No. 134104.
(38) Lavrenova, L. G.; Ikorskii, V. N.; Varnek, V. A.; Oglezneva, I. M.; Larionov, S. V. High-temperature spin transition in coordination compounds of iron(II) with triazoles. *Koordinatsionnaya. Khimiya* **1986**, *12*, 207−215.
(39) Chastanet, G.; Desplanches, C.; Gonidec, M.; Guionneau, P.; Marchivie, M.; Mathonière, C.; Rosa, P. 2.12 - Light-Induced Excited Spin-State Trapping: A Methodological Approach. In *Comprehensive Coordination Chemistry III*; Constable, E. C.; Parkin, G.; Que, L., Jr, Eds.; Elsevier: Oxford, 2021; pp 198−216.

(40) Coelho, A. A. TOPAS and TOPAS-Academic: an optimization program integrating computer algebra and crystallographic objects written in C++. *J. Appl. Crystallogr.* **2018**, *51* (1), 210−218.
(41) Kahn, O.; Codjovi, E.; Garcia, Y.; van Koningsbruggen, P. J.; Lapouyade, R.; Sommier, L. Spin-Transition Molecular Materials for Display and Data Processing. In *Molecule-Based Magnetic Materials*; American Chemical Society, 1996; Vol. *644*, pp 298−310.
(42) Collet, E.; Guionneau, P. Structural analysis of spin-crossover materials: From molecules to materials. *Comptes Rendus. Chim* **2018**, *21* (12), 1133−1151.
(43) Guionneau, P.; Marchivie, M.; Chastanet, G. Multiscale Approach of Spin Crossover Materials: A Concept Mixing Russian Dolls and Domino Effects. *Chem. - Eur. J.* **2021**, *27* (5), 1483−1486.
(44) Salje, E. K. *Phase Transitions in Ferroelastic and Co-Elastic Crystals*; Cambridge University Press: Cambridge, 1991.
(45) Gütlich, P.; Garcia, Y.; Goodwin, H. A. Spin crossover phenomena in Fe(II) complexes. *Chem. Soc. Rev.* **2000**, *29* (6), 419−427.
(46) Kusz, J.; Zubko, M.; Neder, R. B.; Gutlich, P. Structural phase transition to disorder low-temperature phase in $[Fe(ptz)_6](BF_4)_2$ spin-crossover compounds. *Acta Crystallogr. Sect. B* **2012**, *68* (1), 40−56.
(47) Chong, C.; Mishra, H.; Boukheddaden, K.; Denise, S.; Bouchez, G.; Collet, E.; Ameline, J. C.; Naik, A. D.; Garcia, Y.; Varret, F. Electronic and structural aspects of spin transitions observed by optical microscopy. The case of $[Fe(ptz)_6](BF_4)_2$. *J. Phys. Chem. B* **2010**, *114* (5), 1975−1984.
(48) Lakhloufi, S.; Guionneau, P.; Lemée-Cailleau, M. H.; Rosa, P.; Létard, J. F. Structural phase transition in the spin-crossover complex $[Fe(ptz)_6](BF_4)_2$ studied by x-ray diffraction. *Phys. Rev. B* **2010**, *82* (13), No. 132104.
(49) Tolédano, P.; Dmitriev, V. *Reconstructive Phase Transitions in Crystal and Quasicrystals.*; World Scientific, 1996.
(50) Guo, W.; Daro, N.; Pillet, S.; Marchivie, M.; Bendeif, E. E.; Tailleur, E.; Chainok, K.; Denux, D.; Chastanet, G.; Guionneau, P. Unprecedented Reverse Volume Expansion in Spin-Transition Crystals. *Chemistry* **2020**, *26* (57), 12927−12930.
(51) Grosjean, A.; Négrier, P.; Bordet, P.; Etrillard, C.; Mondieig, D.; Pechev, S.; Lebraud, E.; Létard, J. F.; Guionneau, P. Crystal Structures and Spin Crossover in the Polymeric Material $[Fe(Htrz)_2(trz)](BF_4)$ Including Coherent-Domain Size Reduction Effects. *Eur. J. Inorg. Chem.* **2013**, *2013* (5−6), 796−802.
(52) Gufan, Y. M. Theory of phase transition described by two order parameter. *Sov. Phys. - Solid. State* **1980**, *22*, 270−275.
(53) Gufan, Y. M. Phenomenological theory of changes in multicomponent order parameters. *Sov. Phys. - Solid. State* **1980**, *22*, 951−956.
(54) Tongue Magne, G. E.; Keumo Tsiaze, R. M.; Fotué, A. J.; Fai, L. C. Theoretical study of two biquadratically coupled order parameters: Application to two-dimensional multiferroics. *J. Magn. Magn. Mater.* **2020**, *504*, No. 166661.
(55) Imry, Y.; Scalapino, D. J.; Gunther, L. Phase transitions in systems with coupled order parameters. *Phys. Rev. B* **1974**, *10* (7), No. 2900.
(56) Tolédano, J. C.; Tolédano, P. *The Landau Theory of Phase Transitions*; World Scientific Publishing Company, 1987.
(57) Stokes, H. T.; Hatch, D. M.; Campbell, B. J. ISOTROPY Software Suite.
(58) Aroyo, M. I.; Perez-Mato, J. M.; Orobengoa, D.; Tasci, E.; De La Flor, G.; Kirov, A. Crystallography online: Bilbao crystallographic server. *Bulg. Chem. Commun.* **2011**, *43* (2), 183−197.
(59) Landau, L. On the theory of phase transitions. *Ukr. J. Phys.* **2008**, *53*, 25−35.
(60) Janovec, V.; Dvořák, V.; Petzelt, J. Symmetry classification and properties of equi-translation structural phase transitions. *Czechoslovak J. Phys. B* **1975**, *25* (12), 1362−1396.
(61) Carpenter, M. A.; Salje, E. K. H.; Graeme-Barber, A. Spontaneous strain as a determinant of thermodynamic properties for phase transitions in minerals. *Eur. J. Mineral.* **1998**, *10*, 621−691.
(62) Salje, E. K. H.; Carpenter, M. A. Linear-quadratic order parameter coupling and multiferroic phase transitions. *J. Phys.: Condens. Matter* **2011**, *23* (46), No. 462202.
(63) Salje, E. K. H. Ferroelastic Materials. *Annu. Rev. Mater. Res.* **2012**, *42* (1), 265−283.

https://doi.org/10.1021/acs.inorgchem.6c02968
Inorg. Chem. 2026, 65, 19485−19494